Iranian Journal of Veterinary Science and Technology

Received: 2024- Oct- 02
Accepted after revision: 2025- Jun-19
Published online: 2025-Jun-20

RESEARCH ARTICLE

DOI: 10.22067/ijvst.2025.89892.1422

Radioanatomical Study of the Rose-Ringed Parakeet (*Psittacula Krameri*) Head Based on the Findings of Computed Tomography Scanning

Siamak Alizadeh[a], Mohammadreza Hosseinchi[b], Raman Esmaeilnejad[c]

[a] Department of Clinical Sciences, Faculty of Veterinary Medicine, Nag.C., Islamic Azad University, Naghadeh, Iran.
[b] Department of Basic Sciences, Faculty of veterinary medicine, Ur.C., Islamic Azad University, Urmia, Iran.
[c] Doctor of Veterinary Medicine, Faculty of Veterinary Medicine, Ur.C., Islamic Azad University, Urmia, Iran.

ABSTRACT

Computed tomography (CT) is one of the most practical and accurate diagnostic imaging methods for evaluating the bird's head. This study aimed to present the normal anatomical data of Rose-ringed parakeet (Psittacula krameri) head using the CT imaging. In this research, the features of this bird's head were investigated in terms of bones, joints, muscles, sinuses, and other constituent tissues. A retrospective cross-sectional study was conducted on of six adult Rose-ringed parakeet carcasses (3 males and 3 females), aged 1–5 years and weighted between 115–125 g. Following preparing the CT images, the heads underwent gross anatomical studies. Based on the results, reconstructed CT images allowed clear identification of most structures, including the parietal, mandible, occiput, maxillary, preimaxillary, palatine, pterygoid, quadrate, and temporal bones, epithelial membranes, external ear canal and bony labyrinth, ossicles, entoglossal bones, different parts of the infraorbital sinus, brain hemispheres, and various parts of the eyeball and nasal conchae. The results related to the CT evaluation and anatomical examination of the Rose-ringed parakeet's head demonstrated a high correlation. The results of this research provide a valuable reference and can be employ for identifying anatomical features, examining different species of the parakeets, teaching veterinary anatomy, interpreting CT images, and supporting clinical examinations and treatment in this type of parrots.

Keywords

Computed tomography, Head, Radioanatomical, Rose-ringed parakeet (Psittacula krameri)

Abbreviations

CT: Computed Tomography

Number of Figures: 5
Number of Tables: 0
Number of References:: 47
Number of Pages: 14

Corresponding author: *Siamak Alizadeh*
Email: *Si.Alizadeh@iau.ac.ir*
Tel:+98(91)4189-1709

Introduction

Rose-ringed parakeet (Psittacula krameri), is a member of the green parrots (Psittaculidae) family [1]. This parrot is also known as Halsbandsittich (German), Perruche à collier (French), or Cotorra de Kramer (Spanish) [2]. It is similar in appearance to the Alexandrine parakeet (Psittacula eupatria), and it is smaller than the king parrot (Alisterus scapularis), plus lacks the red spots on the edges of its wings [3]. Typically, this parakeet measures approximately 40 cm in body length with a wingspan ranging between 15–17.5 cm. Its weight averages between 115 and 130 g, with males generally being slightly larger than females. In captivity, the species has a life expectancy of 20–30 years, with some individuals living beyond 40 years. The head is normally large and make up about 15–20% of the bird's total body weight [4]. The eyes constitute the bulk of the skull and are placed inside a sclerotic pupil (Figure 1). In some parrot species, the lower part of the eye is surrounded by a unique bony arch or suborbital arch [5]. The rostrum is connected with the skull bone by a joint, which gives the rostrum the ability to move upwards. Furthermore, parrot's tongue is more active and agile due to the entoglossal bones inside the mouth [6]. The mandible and maxilla are placed inside the upper and lower elements of the beak [7]. Inside the upper jaw, nasal cavity, stretched longitudinally aligned turbinates, or conchae. Among the diagnostic imaging techniques, conchae can merely be detected with CT [8]. Parrots also have distinctive facial sinuses, including the primary sinus chamber and the infraorbital sinus, which surround the ventral part of the eyeball and extend to areas around the eyes and ears through a series of canals. Some of these canals, along with the cervicocephalic air sac, extend to the central concha, the lower jaw, and the posterior parts of the neck. Except for the rostral part of the infraorbital sinus, these sinuses can be examined only through CT or magnetic resonance imaging (MRI) [9]. Anatomically, parrots lack the prefrontal, postfrontal, temporal, and postparietal skull bones. Their palatal bones are small and light. These birds lack teeth and have a relatively large and ossified brain chamber, which leads to weight loss and facilitate flight [10, 11]. Domesticated parrots are vulnerable to head injuries, particularly from collisions with window or landing an inappropriate places, which leads to traumatic injuries. In such cases, various imaging techniques can be beneficial in diagnoses. Among these, CT is one of the most accurate and practical diagnostic imaging methods for evaluating head diseases in birds. Previous studies have demonstrated CT's value in avian cranial anatomy. Veladiano et al. (2016) examined the natural anatomy of the heads of blue-and-yellow macaws (Ara ararauna), African gray (Psittacus erithacus), and monks (Myiopsitta monachus) by CT, labeled different parts of their heads on CT images, and finally introduced the obtained findings as an atlas of the natural head anatomy of these parrots [12]. Faillace et al. (2021) applied CT to investigate the anatomical features of the head of the blue-fronted Amazon parrot (Amazona aestiva), and found anatomical variations in some of these features, such as the size and position of the nasal conchae, the infraorbital sinus chamber, the nasopharyngeal duct, and the paraglossum, compared to other parrot species, which can be used in anatomy analysis [13]. Their findings also emphasized the difficulty of examining the inner ear and its related structures and the paratympanic sinus using normal CT images. Thurber et al. (2015) evaluated the differential diagnosis of parrots' neurolog-

Figure 1.
Rose-ringed parakeet (Psittacula krameri)

ical symptoms caused by hydrocephalus syndrome. They concluded that CT is a suitable screening tool for diagnosing hydrocephalus in this type of sick bird [14]. Similarly, Jones et al. (2019) used potassium iodide contrast medium and CT imaging to investigate the radioanatomical characteristics of the rock dove (common pigeon) especially in the head. They found that CT scanning can be utilized as a preferred method for examining different body tissues of this type of bird, and the images obtained with this method will be a valuable source for clinical applications and educational and research purposes [15]. Using CT, Duymus et al. (2013) compared the head anatomy of white, brown, and wild Japanese quails in terms of the head and brain volume, parietooccipital air space volume, and calvarial bone volume and indicated that the head of white quails had the lowest volume values, likely due to genetic differences [16]. Other studies further support and showed the value of CT in the diagnosis of complications and disorders of the head of parrot. Hébert (2019) confirmed Rostroparasphenopalatal luxation in a red-crowned parakeet (Cyanoramphus novaezelandiae) using CT, and the bird completely recovered after therapeutic measures [17]. Krautwald-Junghanns et al. (1998) compared radiology and CT scan techniques in the diagnosis of head diseases in sick parrots and reported the superiority of the CT method in the diagnosis of complications such as bone fractures and identification of hypercalcification or hypocalcification and carcinoma in this area [18]. The investigation of the tomographic features of the head of the Rose-ringed parakeet can be beneficial in identifying anatomical features and evaluating its pathological cases. However, a precise examination of details related to the normal anatomy (morphology and morphometry) of the different parts of this bird's head is necessary. Currently, radioanatomical studies of the head of the Rose-ringed parakeet are rare, and there are no detailed reports in this respect. Accordingly, this study aimed to investigate the normal anatomy of the Rose-ringed parakeet's head by CT using three-dimensional (3D) modeling.

Result

Reconstructed CT images revealed that most structures of the head of the Rose-ringed parakeet (Psittacula krameri) were identifiable. In the 3D images, the parrot's head appeared rounded and compact. The jugal arch and the palatine bone were fused in the remaining parts of the skull, except for the cranial facial bones. Even small bones of the head, such as ear bones and entoglossal bones inside the mouth, could also be evaluated in these CT images. Using the lung window filter, it was possible to observe the bony trabecular in the head. This setting also enabled evaluation of the parietal and temporal bones, nasal conchae, epithelial membranes, the external ear canal, and bony labyrinth. Further, with covering tissues, different parts of the infraorbital sinus could be observed using this filter. Furthermore, different soft tissue windows were adjusted to allow for the identification of brain hemispheres, the cerebellum, optic nerve, pupil muscles, and eye lenses (Figures 3-5). Based on the findings, the columella ossicle, its external cartilage, and the cochlea were not detectable on CT. The eyeballs of all parrots were complete and bony and located on the skull's lateral side (Figure 3i). The mandible appeared bony and lacked a distinct symphysis (Figures 3b and 4a), while the rostrum was keratinous, large, and ventrally curved. The operculum was observed on the dorsal base of the nostrils. Bones such as occipital, maxillary, premaxillary, mandible, palatine, pterygoid, and quadrate were pneumonized and had air bubbles. The nasal cavities were divided by a septum, which thickened slightly from the rostral to the caudal side. Its caudal third was cartilaginous, while the middle third and the rostral were bony. The ectethmoid, mesethmoid, maxillary, and preimaxillary bones were involved in the formation of the nasal cavity, and the nasal cavity comprised three parts: olfactory, respiratory, and vestibular. Each nasal cavity had a single duct with caudal, middle, and rostral cartilaginous conchae. The rostral concha C-shaped and located in the vestibular part of the nasal cavity decreased in thickness from the rostral to the caudal direction and contained a basal lamella along the lateral nasal cavity wall. The middle concha was in the form of long ducts that originated from a basal lamella and was located in the upper respiratory tract of the nasal cavity. This lamella also splits into a sinusoidal and a spiral lamella. The spiral lamella extended to the entrance of the nasopharyngeal canal. The caudal concha, smaller and hollow, was located at the nasal cavity's rear. The nasal and oral cavities were connected through the nasopharyngeal canal (Figures 4c and 5h), which connected the maxilla-palatal process and the palatine bone's choanal part from the rostro-lateral and caudal sides. The caudal part of this duct linked with the interorbital septum (Figures 4e and 5f). The oral cavity included the palatal, mandible, premaxillary, and maxillary bones, along with associated muscles and tongue. These bones, along with the pterygoid, contributed to pharynx formation (Figures 5c-d). The choana was located in the dorsal part of the pharynx and oral cavity and connected the oral cavity to the nasal cavity (Figure 3g). The tongue was strong and large, and could be identified in the CT images, located in the middle third and caudal of

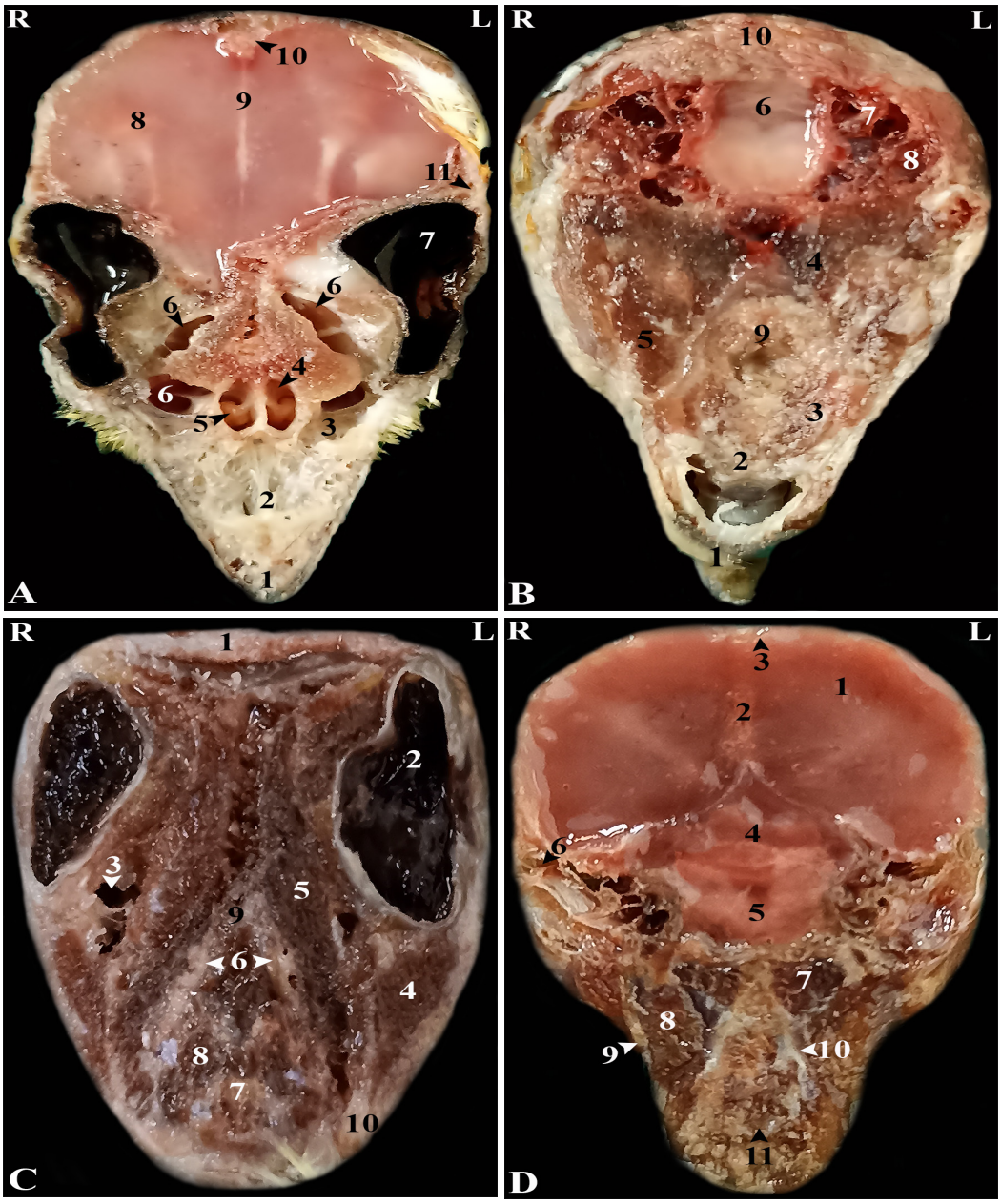

Figure 2.
Representative photographs of anatomic cross sections of the adult cockatiel (Nymphicus hollandicus) head. A (level of the Eye) and B (level of the external acoustic meatus) in the dorsal plane and C (level of the rostral border of the orbital fossa) and D (level of the external acoustic meatus) in the transverse plane. A: (1) Rampheteca, (2) Premaxilla bone, (3) Maxilla bone, (4) Left nasal cavity, (5) Caudal nasal concha, (6) Infraorbital sinus, (7) Eye, (8) Brain hemispheres, (9) Falx cerebri, (10) Occipital bone, (11) Temporal bone. B: (1) Rampheteca, (2) Premaxilla bone, (3) Palatine bone, (4) Ethmomandibularis muscle, (5) Pterygoideus muscle, (6) Cerebellum, (7) Bony labyrinth, (8) External acoustic meatus, (9) Caudal nasal concha, (10) Occipital bone. C: (1) Fronto-parietal bone, (2) Eye, (3) Infraoebital sinus, (4) Pterygoideus muscle, (5) Ethmomandibularis muscle, (6) Hard Palate, (7) Eye, (8) Caudal nasal concha, (9) Lingual process of hyoid bone, (10) tongue, (11) Choanal cleft, (12) Mandible. D: (1) Cerebrum, (2) Falx cerebri, (3) Occipital bone, (4) Brain stem, (5) Chiasma optic, (6) External acoustic meatus, (7) Ethmomandibularis muscle, (8) Pterygoideus muscle, (9) Mandible, (10) Hard palate, (11) Lingual process of hyoid bone. R, Right; L, Left.

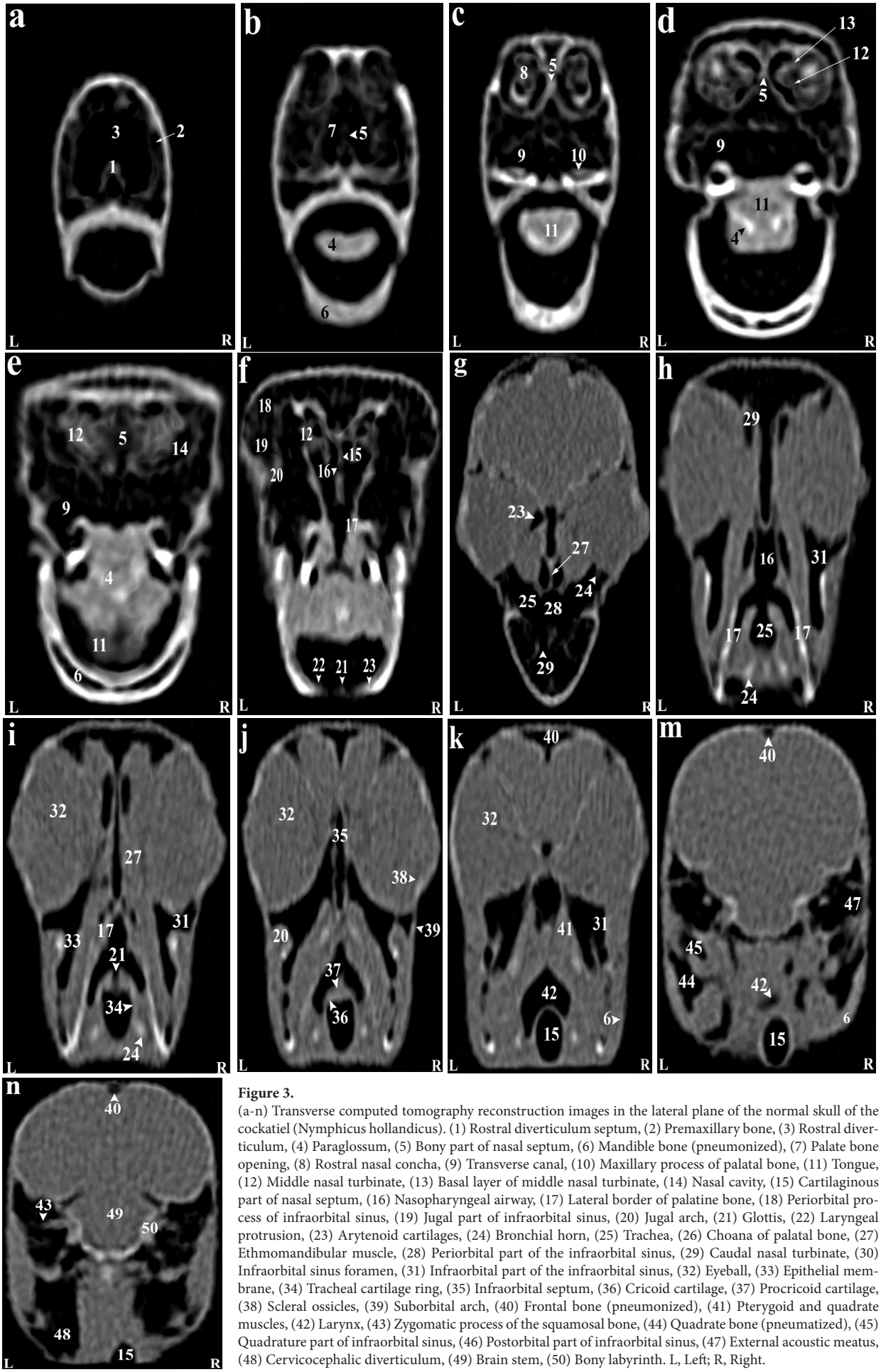

Figure 3.
(a-n) Transverse computed tomography reconstruction images in the lateral plane of the normal skull of the cockatiel (Nymphicus hollandicus). (1) Rostral diverticulum septum, (2) Premaxillary bone, (3) Rostral diverticulum, (4) Paraglossum, (5) Bony part of nasal septum, (6) Mandible bone (pneumonized), (7) Palate bone opening, (8) Rostral nasal concha, (9) Transverse canal, (10) Maxillary process of palatal bone, (11) Tongue, (12) Middle nasal turbinate, (13) Basal layer of middle nasal turbinate, (14) Nasal cavity, (15) Cartilaginous part of nasal septum, (16) Nasopharyngeal airway, (17) Lateral border of palatine bone, (18) Periorbital process of infraorbital sinus, (19) Jugal part of infraorbital sinus, (20) Jugal arch, (21) Glottis, (22) Laryngeal protrusion, (23) Arytenoid cartilages, (24) Bronchial horn, (25) Trachea, (26) Choana of palatal bone, (27) Ethmomandibular muscle, (28) Periorbital part of the infraorbital sinus, (29) Caudal nasal turbinate, (30) Infraorbital sinus foramen, (31) Infraorbital part of the infraorbital sinus, (32) Eyeball, (33) Epithelial membrane, (34) Tracheal cartilage ring, (35) Infraorbital septum, (36) Cricoid cartilage, (37) Procricoid cartilage, (38) Scleral ossicles, (39) Suborbital arch, (40) Frontal bone (pneumonized), (41) Pterygoid and quadrate muscles, (42) Larynx, (43) Zygomatic process of the squamosal bone, (44) Quadrate bone (pneumatized), (45) Quadrature part of infraorbital sinus, (46) Postorbital part of infraorbital sinus, (47) External acoustic meatus, (48) Cervicocephalic diverticulum, (49) Brain stem, (50) Bony labyrinth. L, Left; R, Right.

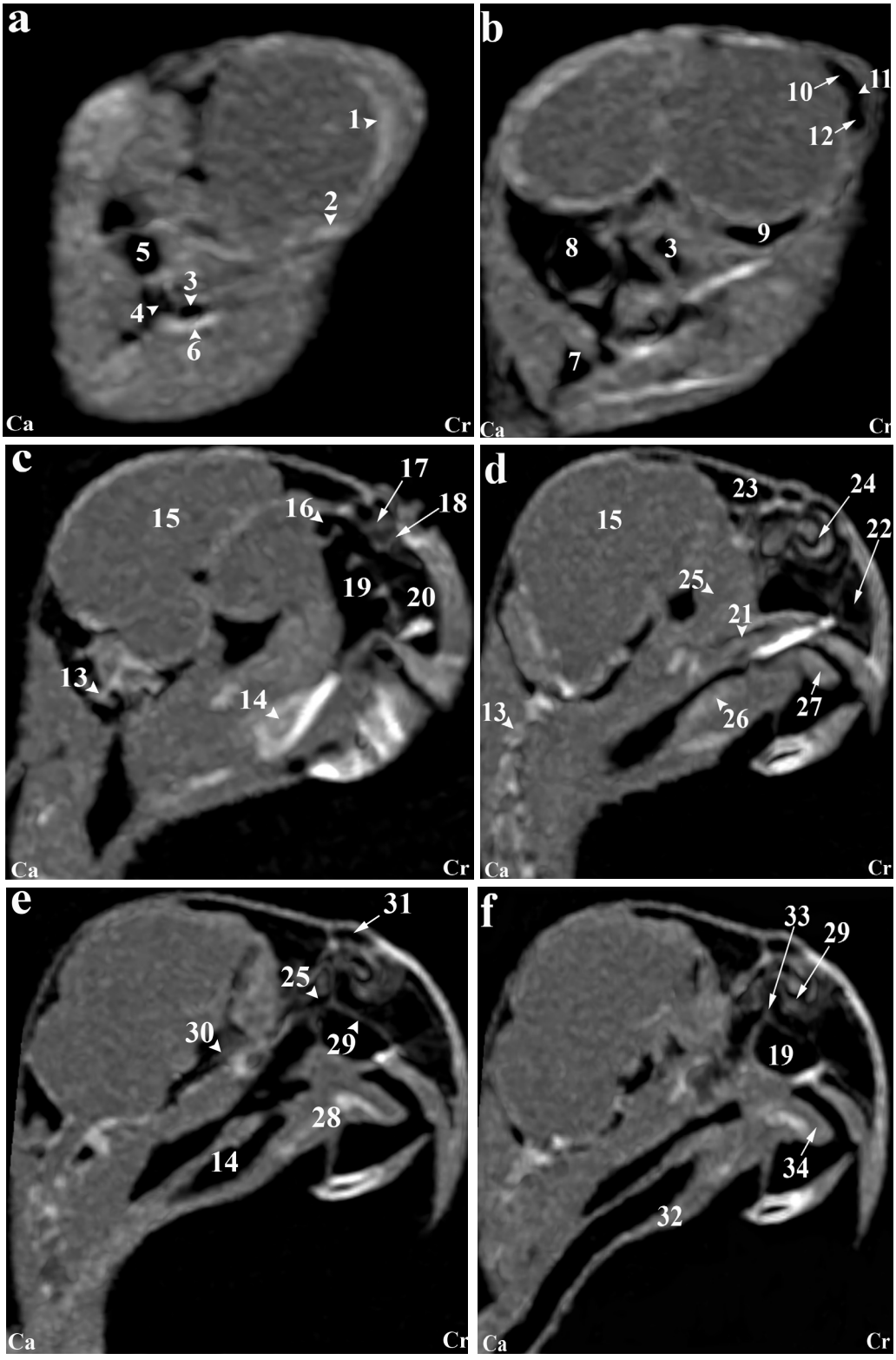

Figure 4.
(a-f) Sagittal computed tomography reconstruction images (lateromedial plane) of the normal skull of the cockatiel (Nymphicus hollandicus). (1) Scleral bones, (2) Suborbital arch, (3) Postorbital part of the infraorbital sinus, (4) Quadrate bone (pneumonized), (5) External ear foramen, (6) Mandible bone, (7) Cervicocephalic diverticulum, (8) Occipital bones (pneumonized), (9) Infraorbital part of infraorbital sinus, (10) Periorbital process, (11) Epithelial membrane, (12) Jugal portion of infraorbital sinus, (13) Cervical vertebrae, (14) Trachea, (15) Encephalon of the brain, (16) Caudal nasal turbinate, (17) Middle nasal turbinate, (18) Rostral nasal turbinate, (19) Transverse canal, (20) Premaxillary bone (pneumonized), (21) Palate bone (pneumonized), (22) Rostral diverticulum, (23) Frontal bone (pneumonized), (24) Nasal cavity, (25) Nasopharyngeal airway, (26) Larynx, (27) Paraglossum, (28) Basihyal, (29) Bony part of nasal septum, (30) Infraorbital septum, (31) Nostril, (32) Tracheal rings, (33) Cartilaginous part of nasal septum, (34) Tongue. Ca, Caudal; Cr, Cranial.

the inferior part of the oral cavity (Figures 3c-d). The oral cavity had a hyobranchial apparatus. The tongue's base was in close contact with the paraglossum and the cranial part of the basihyal. Bishyal processes and uhorial bones were detectable in the trachea's larynx and cranial part. The branchial horn (caudal part of the hyobranchial apparatus) was located in the inner part of mandible's ramus, or tracheal cranial part. Its caudal third was associated with mandible masseter muscles. The larynx consisted of a ring-shaped cricoid cartilage and two pyramid-shaped arytenoid cartilages. The results of the current study demonstrated that the procricoid cartilage was located within the middle part of the cricoid cartilage and formed the larynx 's dorsocaudal part (Figures 3b-j). The glottis was centrally placed in the larynx and surrounded by arytenoid cartilages. While laryngeal mounds (Mons laryngealis) were visible in CT cross-sectional. The place where the cricoid joins the tracheal cartilages also appeared ring-shaped in these images (Figures 3f and 5f).

The entire pupil cavity was filled with an oval eyeball bordered externally by the frontal bone and suborbital arch. A bony trabecular septum separated the pupils. All parrots under study had a complete bony eyeball (Figures 3j and 5h). In the obtained CT images, the eye lens was not clearly detectable, and the cranial chamber (aqueous) and the caudal (vitreous) were not distinguishable. The retina was unrecognizable. Eyeball muscles, lacrimal glands, and the third eyelid (nictitating membrane) had similar attenuation values and were indistinguishable. Scleral bones appeared as two indistinct lines on cross-sections images and as circular or round in sagittal images (Figures 3j, 4a, and 5h).

The parakeet's encephalon could be evaluated in the CT images (Figures 4c and 5i). Although, brain hemispheres such as the telencephalon and diencephalon, along with the brainstem and cerebellum, were well identified and could be distinguished from each other in cadavers, they shared similar attenuation in CT, making them difficult to differentiate. The findings revealed that the external acoustic meatus and the external opening of the ear were recognizable in CT images (Figures 3m and 5c), but the tympanic membrane was not visible in either CT images or carcasses examinations. Hence, different parts of the middle ear were not distinguishable. Nonetheless, the presence of low-resolution lines in the distal third of the external acoustic meatus can demonstrate parts of the middle ear such as infraorbital (columella) and extracolumella cartilage. The bony labyrinth of the inner ear was clearly visible in both in the cadaver samples and CT images.

Based on our findings, the paratympanic sinus could not be identified in CT images. Muscles of the head were only faintly visible hyperattenuated lines. Larger muscles, such as quadrate, pterygoid, and ethmomandibular, were somewhat distinguishable, although the jaw adductor muscle despite its size, was poorly detectable in CT images (Figures 3g and 5c). The infraorbital sinus was surrounded by skull bones and covering and muscular tissues and was found as a large triangular cavity that covered a large part of the head. The premaxillary bone was located in the rostral part of this sinus, with palatine and pterygoid bones located in its inner part. Further, the quadrate, jugal arch, and mandible were located in the lateral part. This sinus included the rostral diverticulum, transverse canal, postorbital, preorbital, infraorbital, quadrate bones, cervicocephalic diverticulum, and mandibular recess. The rostral diverticulum and the transverse canal were single, and the remaining parts were in pairs. Except for the periorbital parts, the transverse canal, and the rostral diverticulum, the remaining parts of the suborbital sinus were covered by the masticatory muscle (Figures 3-5). The rostral diverticulum, extending along the premaxillary bone, was divided into two parts by a thin bony septum, which gradually thinned from rostral to the caudal direction, and eventually disappeared in the middle parts of the diverticulum. The transverse canal was a short and horizontal passage. The maxillary process of the palatine bone and the upper jaw-palatine process (maxillopalatine) of the maxilla, were located in this canal's ventral and distal parts, respectively. This canal connected the periorbital region and rostral diverticulum (Figures 3a, 4d, and 5h). The nasopharyngeal duct divided the periorbital region into left and right parts. The jugal portion was connected dorsally to the periorbital region, ventrally to the choanal part of the palatine bone, and laterally to the jugal arch. A relatively thin epithelial layer separated the periorbital and the jugal portion. These subdivisions were connected in the caudal part, near the infraorbital part of the infraorbital sinus. The infraorbital part, the largest part, covered a large area of the ventral surface of this sinus and extended to the eyeball. It connected to the palatine bone and interorbital septum from the medial part and to the suborbital and jugal arches from the lateral part. The infraorbital and postorbital parts were directly connected. The infraorbital and postorbital parts were the largest parts of the infraorbital sinus, respectively. The postorbital part was located in the pterygoid's lateral part, the zygomatic process's internal part, and the jugal bow's posterior part, which was connected with the musculature. The masseter, pterygoid, quadrate, and temporal muscles were located in the postorbital area. The caudoventral part of postorbital was connected to the quadrate por-

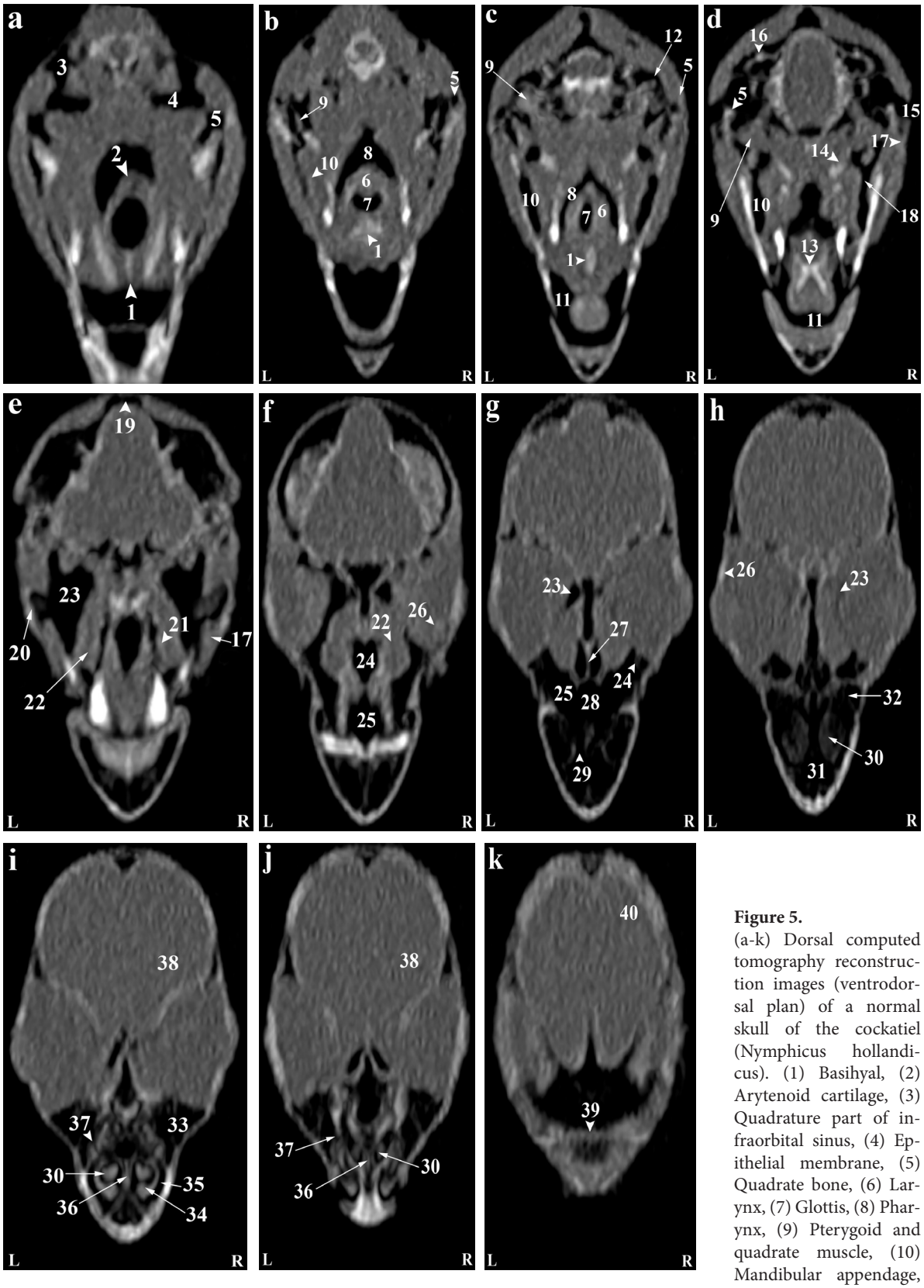

Figure 5.
(a-k) Dorsal computed tomography reconstruction images (ventrodorsal plan) of a normal skull of the cockatiel (Nymphicus hollandicus). (1) Basihyal, (2) Arytenoid cartilage, (3) Quadrature part of infraorbital sinus, (4) Epithelial membrane, (5) Quadrate bone, (6) Larynx, (7) Glottis, (8) Pharynx, (9) Pterygoid and quadrate muscle, (10) Mandibular appendage, (11) Oral cavity, (12) External acoustic meatus, (13) Paraglossum, (14) Pterygoid bone, (15) External ear foramen, (16) Bony labyrinth, (17) Jugal arch, (18) Postorbital part of infraorbital sinus, (19) Occipital bones (pneumonized), (20) Suborbital arch, (21) Palate bone, (22) Ethmomandibular muscle, (23) Infraorbital part of the infraorbital sinus, (24) Nasopharyngeal canal, (26) Scleral ossicles, (27) Infraorbital septum, (28) Cartilaginous part of the nasal septum, (29) Palate foramen, (30) Middle nasal turbinate, (31) Rostral diverticulum, (32) Cranial foramen of eyeball, (33) Preorbital part of the infraorbital sinus, (34) Rostral nasal turbinate, (35) Nasal cavity, (36) Bony part of nasal sinus, (37) Infraorbital sinus foramen, (38) Encephalon, (39) Craniofacial flexion, (40) Frontal bone. L, Left; R, Right.

tion. The smallest part of the infraorbital sinus was related to a quadrate part, which was laterally connected to the quadrate bone. The mandibular recess and cervicocephalic diverticulum were linked to the postorbital part. The mandibular recess was visible in the inner and rostral parts of the mandibular ramus. In fact, this recess was located in the inner part of the postorbital and the ventral part of the infraorbital canal. Lastly, the cervicocephalic diverticulum was detectable and extended to the cervical region (Figures 3n and 4b).

Discussion

In this study, we aimed to investigate the normal anatomy of the Rose-ringed parakeet (Psittacula krameri) head using computed tomography (CT). Based on our results, reconstructed CT images successfully allowed the identification of most skeletal and soft tissue structures of the head, including parietal, temporal, and maxillary bones, ossicles, nasal conchae, infraorbital sinus subdivisions, encephalon, and ocular components. The CT findings showed a high correlation with gross anatomical observations, demonstrating that CT is a practical and accurate method for describing the radioanatomical features of this parrot's head.

The CT and gross anatomy results in this study revealed that the skull of the Rose-ringed parakeet (Psittacula krameri) shares similarities with other parrot species, with no observable difference between the skulls of male and female individuals. CT diagnostic method enabled the anatomical description of the skull, aligning with the reports of some researchers in this field [19, 20]. Despite the small size of the parakeet's head, high quality images were obtained, allowing for clear identification of bones and tissues of the head, such as the jugal arch, palatine bone, ear ossicles, and antoglossum bones inside the mouth and different parts of the infraorbital sinus. Of course, the quality of these images was significantly influenced by the type of CT scanner used (Toshiba Multi-slice CT scanner Asteion Premium 4, Model: TSX-021B, Japan). In this research, the bony trabeculae of the head of the Rose-ringed parakeet were observed by using a suitable window (WW: 2336 HU; WL: 368 HU), the study successfully visualized parietal and temporal bones, nasal conchae, epithelial membranes, external acoustic meatus, and bony labyrinth. Performing head CT in sagittal, transverse, and dorsal planes, were obtained allowing detailed assessment of individual anatomical components, particularly the infraorbital sinus. Scanning the head in different planes solved the problem of superimposition of the images of different tissues, and each of the tissues was individually and specifically evaluated accordingly. These observations are supported by Cubo and Casinos (2000), thay examined the bones of different bird species and reported that some bird bones contain air bubbles [21]. In this study, some of the skull bones, such as the occipital, maxillary, preimaxillary, mandible, palatine, pterygoid, and quadrate bones, are trabecular and pneumonized and have air bubbles. However, Veladiano (2018) investigated the head CT of different birds and described the role of the pneumatic foramen, suborbital and paratympanic sinuses [22], which contradicts our findings. In our scans, the pneumatic foramen was undetectable, and the origin of bone pneumatization could not be evaluated. Furthermore, the paratympanic sinus was not visible , probably due to the fusion with middle ear tissues.

In this study, the tympanic membrane and different parts of the middle ear were also not visible in the CT images. However, the presence of low-resolution lines within the distal third of the external acoustic meatus can demonstrate parts of the middle ear, such as columella and extracolumella cartilage. These results are consistent with Wild's study (2015) [23].

According to our CT images, the tympanic membrane and different parts of the middle ear were not visible. These results are in agreement with Wild's study (2015), which reported that the cochlea, tympanic membrane, extracolumella cartilage, and columella of parrots are extremely small and therefore cannot be observed in CT images. It has been reported that the cochlea, tympanic membrane, extracolumella cartilage, and columella of parrots are extremely small and thus cannot be observed in CT images. Nonetheless, it is suggested that other diagnostic imaging methods, such as micro-CT and MRI, be used to evaluate these parts.

Our findings regarding nasal cavity conchae align with studies reporting three conchae per cavity in birds [24, 25]. The results of the current study revealed that in Rose-ringed parakeet, each nasal cavity, contained of a single meatus with caudal, middle, and rostral cartilaginous conchae. Other species, like the Congo gray parrot (Psittacus erithacus) [26], the budgerigar (Melopsittacus undulates) [27], and the brown-eared nightingale (Hysipetes amaurotis) [28], have been reported to possess only two conchae, while some like petrel (Pagodroma sp.) have more than three [29]. In our study , the middle and caudal turbinates had the largest and smallest sizes, respectively, consistent with the results of other parrot studies done by Hanafy (2021) and Al-Rubaie and Kadhim (2023) [25, 30]. In the skull of the Rose-ringed parakeet, similar to other parrots, the middle concha resembled a long duct,

which is located in the upper respiratory airway and originates from a basal lamella, which itself is divided into a sinus lamella and a spiral lamella. Moreover, the caudal concha is small and hollow and is placed in the caudal nasal cavity. Contradictory findings were reported by Faillace et al. (2021), who examined the CT results of the nasal conchae of the blue-fronted Amazon parrot (Amazona aestiva), described the middle concha as a narrow linear structure inside the rostral concha [13]. They further found that in this type of parrot, the caudal concha can have different sizes, so that the size of this concha is large in some of these birds, while it is extremely small in others. In a study, Madkour (2019) suggested the presence of bone tissue in addition to cartilaginous tissue within nasal conchae of some bird species [31]. Madkour's report does not match the result of our study, according to our observations, the structure of the nasal conchae of the Rose-ringed parakeet was purely cartilaginous, and this finding was confirmed by the attenuation of the CT images of the head. Van Zeeland (2018) investigated the upper respiratory tracts of parrots and reported that the nasopharynx contains adenoids and lymphoid tissues and connects the nasal cavities and the throat [32]. The Van Zeeland's study is somewhat in line with our gross anatomy results. The nasal and oral cavities were linked through the nasopharyngeal duct in the Rose-ringed parakeet. Based on CT images, the nasopharyngeal duct was rostrolaterally and caudally connected to the maxilla-palatal process of the maxillary bone and the choanal part of the palatine bone, respectively. The caudal part of the nasopharyngeal duct was linked to the interorbital septum. Unfortunately, we found no valid literature on the nasopharyngeal CT characteristics of birds and because of that we couldn't compare our results on that with other studies.

The Rose-ringed parakeet oral cavity had a hyobranchial apparatus, with its caudal part located in the inner part of the mandible's ramus, in other words, cranial part of trachea. These findings conform to the results of other studies performed on parrots. According to our observations, the tongue's base was in close contact with the paraglossum and the cranial part of basihyal.

Our results also demonstrated that the pupil of the Rose-ringed parakeet is completely bony. In the gross anatomy studies, it was possible to determine the anterior and caudal chambers, lens, and optic nerve of this bird's eye, which matches the reports of most researchers, and it seems that the eye anatomy of this type of parrot does not particularly differ from that of other birds [33]. However, unlike the gross anatomical evaluations, the lens was not clearly visible, and it was impossible to distinguish the ocular chambers in the obtained CT images. The retina, eyeballs' muscles, lacrimal glands, and third eyelid (nictitating membrane) were indistinguishable and therefore could not be separated from each other. The researchers of this study could not find written and specific reports about CT scans of birds' eyes and compare them with the results of our study. However, according to the findings of our study, we recommend the use of diagnostic imaging methods such as ultrasonography, micro-CT, MRI, and other specialized eye evaluation methods for examining the internal tissues of the eye.

In the CT images, while, the masticatory muscle could be identified due to their large size, other head muscles, including eyeball's muscles, and even nerve vessels showed highly close attenuation, and it was difficult to distinguish between them; thus, they did not undergo separate analyses. Different radiation factors were employed to increase the clarity and contrast of these tissues, but no suitable answer was obtained in this regard.

Based on anatomical examination of the budgerigar and Casco (African grey parrot), Smallwood (2014) reported that the cricoid cartilage of the larynx of these birds is wide and has a rostral process [34]. In another study, Silva et al. (2020) found that the cricoid cartilage of the larynx of the cockatiel is smooth and small and has two rostral and lateral processes [35], which contradicts our findings. In contrast to the findings of both Smallwood (2014) and Silva et al. (2020), our study showed that in the Rose-ringed parakeet, the larynx consisted of an annular cricoid cartilage and two pyramidal arytenoid cartilages, with a smooth and thin cricoid cartilage lacking processes. Additionally, a procricoid cartilage was present in the middle part of the cricoid, forming the dorsocaudal portion of the larynx.. In the Rose-ringed parakeet, the larynx consisted of an annular cricoid cartilage and two pyramidal arytenoid cartilages. The cricoid cartilage was smooth and thin and had no processes. In the middle part of the cricoid cartilage, there was the procricoid cartilage, which formed the dorsocaudal part of the larynx.

Although several studies, have examined the anatomy of the infraorbital sinus in some poultry such as hens, turkeys, and geese [36], there is no detailed and comprehensive report about the anatomy and CT features of the infraorbital sinus in parrots. Our research showed that in the Rose-ringed parakeet, the infraorbital sinus was surrounded by skull bones and covering and muscular tissues, and in the CT images, it was detected as a large triangular cavity that covered a large part of the head. The premaxillary bone was located in the rostral part, the palatine and pterygoid bones were located in its inner part, and the quadrate bone, jugal arch, and mandible bones were located in

the lateral part of this sinus. Grist (2006) conducted an anatomical study on domestic chickens and found that there were fewer infraorbital sinus chambers in the head of this type of bird [37], though he did not named and characterize these chambers. Eventually, it was indicated that this sinus is shorter in other birds and is limited by the infraorbital part. According to our observations, this sinus included the rostral diverticulum, transverse canal, postorbital, preorbital, infraorbital, and quadrate parts, cervicocephalic diverticulum, and mandibular recess in the Rose-ringed parakeet. The head and neck of this type of parrot were widely pneumatized with this sinus. No specific homologies were inferred in this regard since the analogy of the infraorbital sinus and phylogenetic evaluations between the Rose-ringed parakeet and other parrots was impossible.

Massari et al. (2020) performed CT on the head of a macaw and reported that the infraorbital, periorbital, and rostral diverticulum of the infraorbital sinus can be easily detected, which is mainly due to the large chambers of this sinus and the absence of covering muscles in this region [38]. It was further indicated that the postorbital, quadrate, and mandibular recess parts were not detectable because they were small and superimposed by the masticatory muscle. These findings somewhat corroborate the results of our study. Based on our findings in the Rose-ringed parakeet, except for the periorbital, transverse canal, and rostral diverticulum, the remaining parts of the suborbital sinus were covered by the masticatory muscle.

In some studies, the existence of a paratracheal recess was reported in Amazon and Cockatoo [39], as well as Anodorhynchus and Ararauna macaws [40], but we found no such structures in the Rose-ringed parakeets; therefore, this feature can be mentioned in the comparative anatomy of this type of parrot.

The skull of the Rose-ringed parakeet was relatively small, and the limit distance of its constituent bones was visible. The periorbital sinus was located in the anterorbital fenestra, and the zygomatic process of the squamosal bone surrounded the postorbital sinus. CT images showed head muscles as hyper-attenuated lines and not very clear. However, relatively larger muscles such as quadrate, pterygoid, and ethmomandibular were somehow distinguishable. The jaw adductor muscle, although large, it could not be detected in the CT images, and its boundaries was determined based on the topography of the bones in that region.

Finally, the columella ossicle, its external cartilage, and cochlea were not recognizable in CT images likely due to their small size. Hence, it is recommended that other diagnostic imaging methods such as micro-CT or MRI be utilized in cases where it is intended to evaluate these structures.

Overall, this study demonstrates that the skull of the Rose-ringed parakeet is not that much different from that of other parrots. The only morphological differences were related to some parts of the nasal cavity, infraorbital sinus, and, to some extent, the hyobranchial apparatus and nasopharyngeal duct.

In conclusion, the CT scan is one of the most effective and non-invasive diagnostic imaging methods to describe and dissect most of the hard and soft tissues of the Rose-ringed parakeet's head. The results of this study demonstrated its utility on examining the infraorbital sinus and the turbinates, or conchae, of nasal cavities. The investigation of the tomographic features of the Rose-ringed parakeet's head can be useful in identifying anatomical features and evaluating its pathological cases. The results of this research can be utilized as a standard reference and atlas for identifying anatomical characteristics, examining various species of Rose-ringed parakeets, teaching anatomy, and interpreting CT scan images. Moreover, these findings can be used for clinical examinations and aid in treatment of this type of parrot.

Materials and Methods

Ethical consideration

This work involved the use of procedures that did not differ from established internationally recognized high standards (best practice) of veterinary clinical care for the individual animals. The study was approved by the Ethical Committee of Islamic Azad University, Urmia, under registration code Ir.iau.urmia.rec.1403.038

Study design and Specimens

The current retrospective cross-sectional study was conducted using carcasses of six adult Rose-ringed parakeets (Psittacula krameri) (3 males and 3 females) with an average age range of 1–5 years and an average weight between 115–125 g. These birds were well-nourished during their lifetime. The carcasses were collected from a private Rose-ringed parakeet breeding facility in Tehran and stored at -20°C until use. The parrots, which previously died for various reasons, were used in this study, and the cause of their deaths was unrelated to this study. Maturity of the specimens was confirmed by factors such as assessing neck ring coloration, the amount of scales on the feet, the condition of the feathers, and the beak color. Sex of the specimens was also determined following a necropsy of the carcass [41, 42].

Computed tomography (CT) studies

For CT imaging, each parrot was placed on the scanner table in a sternal recumbent position, with the head oriented forward and the mandible aligned perpendicular to the gantry. Scanning was performed in the sagittal, transverse, and dorsal planes with a thickness and interval of 1 mm. A helical scanner (Toshiba Multislice CT Scanner Asteion Premium 4, Model: TSX-021B, Japan) was employed for CT. In addition, appropriate windows were selected to examine soft and bone tissues. The technical factors of the CT scanner included gantry rotation time (400 ms), slice thickness (1 mm), reconstruction distance (0.5–1 mm), pitch ratio

(1), kVp (120), mAs (10), physical detector collimation (32 × 0.6 mm), final section collimation (64 × 0.6 mm), resolution (512 × 512 pixels), and resolution range (0.92 × 0.92), Kernel (10 H), and increment (0.5 mm) [13, 43]. Imaging was performed based on the above-mentioned factors, and the obtained images were saved in DICOM format [44].

Three-dimensional reconstruction

DICOM images were imported to a computer system equipped with 3D modeling software (Onis CT software, Multi-Modality Workplace: VE 2.5A) and displayed using bone window settings (window width: UH 4500 and window level: UH750), consistent with previous research [45]. Further analyses was performed using 3D slicer software [46]. Based on our observations, this technique allowed the use of lung (WW: 2336 HU; WL: 368 HU) and bone (WW: 950; WL: 390) windows, thus providing high-resolution images of the tissues and structures that constitute the head region of the parrots.

Anatomical studies

Following CT imaging, each frozen parrots head was transversely sectioned using an electric band saw at 5 mm intervals, from the rostral part of the rhamphotheca to the anterior end of the neck. Each slice was rinsed with water and cleaned with a soft brush and photographed. Visible textures and structures were identified and labeled on these photographs. Further, CT images were matched with these photos and labeled accordingly. Nomina Anatomica Veterinaria guidelines was used as the obtained scientific term [47] (Figure 2).

Authors' Contributions

Conceived and designed the experiments: SA, MRH. Performed the experiments: MRH. Analyzed the data: SA, MRH, RE. Research space and equipment: SA, MRH. Contributed reagents/materials/analysis tools: SA. wrote the paper: SA, MRH.

Acknowledgements

The authors thank the Vice Chancellor for Research of Islamic Azad University of Urmia for financial supports (Protocol Code: 3/ 29801).

Competing Interests

The authors declare that there is no conflict of interest.

Reference

1. Abed SA, Salim MA, Alsaffah SM. First record of Alexandrine Parakeet psittacula eupatria (Psittaculidae, psittaciformes)(Linnaeus 1766) in Iraq. Indian Journal of Ecology. 2020;47(3):887-8.

2. Braun M. Die Bestandssituation des Halsbandsittichs Psittacula krameri in der Rhein-Neckar-Region (Baden-Württemberg, Rheinland-Pfalz, Hessen), 1962-2008, im Kontext der gesamteuropäischen Verbreitung. Vogelwelt. 2009;130:77-89.

3. Şahin D, Arslangündoğdu Z. Breeding status and nest characteristics of roseriged (Psittacula krameri) and alexandrine parakeets (Psittacula eupatria) in Istanbul's city park. Applied Ecology & Environmental Research. 2019;17(2). Doi: 10.15666/aeer/1702_24612471.

4. Mentil L, Monti P, Fraticelli F, Carpaneto GM. A morphometric sexing approach for the Ring-necked Parakeet Psittacula krameri in Italy. Ringing & Migration. 2018;33(2):64-7. Doi: 10.1080/03078698.2018.1631609.

5. Henley E. A bird's eye view of breakdown in parrot–caregiver relations. Companion Animal. 2018;23(2):104-8. Doi: 10.12968/coan.2018.23.2.104.

6. Benedict L, Charles A, Brockington A, Dahlin CR. A survey of vocal mimicry in companion parrots. Scientific Reports. 2022;12(1):20271. Doi: 10.1038/s41598-022-24335-x.

7. Forouzan P, Cohen PR. Parrot Beak nail: case report and review of parrot beak nail dystrophy. Cureus. 2021;13(6). Doi: 10.7759/cureus.15974.

8. Langlois I, Barrs VR, Dufresne PJ. Corrigendum to 'Rhinitis due to Aspergillus pseudoviridinutans in an orange-winged Amazon parrot (Amazona amazonica)'[Med. Mycol. Case Rep. 30 (2020) 46–50]. Medical Mycology Case Reports. 2021;33(4):38-55 Doi: 10.1016/j.mmcr.2020.11.001.

9. Faux CM, Logsdon ML. Infraorbital sinusitis. Comparative Veterinary Anatomy: Elsevier; 2022;11(2):1264-70.

10. Hollwarth AJ, Esmans MC, Herrmann A, Dutton TA. Heterotopic Ossification Bone Formation in the Frontal Bones of an African Grey Parrot (Psittacus erithacus). Journal of Avian Medicine and Surgery. 2023;36(4):388-93. Doi: 10.1647/22-00002

11. Carril J, Tambussi CP, Degrange FJ, Benitez Saldivar MJ, Picasso MBJ. Comparative brain morphology of Neotropical parrots (Aves, Psittaciformes) inferred from virtual 3D endocasts. Journal of anatomy. 2016;229(2):239-51. Doi: 10.1111/joa.12325

12. Veladiano IA. Tomographic imaging in companion avian species. 2018;13(2):655-666.

13. Faillace ACL, Vieira KRA, Santana MIS. Computed tomographic and gross anatomy of the head of the blue-fronted Amazon parrot (Amazona aestiva). Anatomia, Histologia, Embryologia. 2021;50(1):192-205. Doi: 10.1111/ahe.12618.

14. Thurber MI, Mans C, Fazio C, Waller K, Rylander H, Pinkerton ME. Antemortem diagnosis of hydrocephalus in two Congo African grey parrots (Psittacus erithacus erithacus) by means of computed tomography. Journal of the American Veterinary Medical Association. 2015;246(7):770-6. Doi: 10.2460/javma.246.7.770.

raphy and computed tomography in evaluating the heads of psittacine and raptorial birds. Journal of Avian Medicine and Surgery. 1998;149-57.

19. Sabat D, Millan S, Suchismita Sethy P, Marathe S, Sahoo H, Mishra M, editors. Elemental analysis of various feathers of Indian Rose Ringed Parakeet Psittacula krameri. Acta Biology. 2017;14(3):47-66. Doi: 10.1007/978-3-319-46601-9_5.

20. Iwaniuk AN, Dean KM, Nelson JE. Interspecific allometry of the brain and brain regions in parrots (Psittaciformes): comparisons with other birds and primates. Brain Behav Evol. 2004;65(1):40-59. Doi: 10.1159/000081110.

21. Cubo J, Casinos A. Incidence and mechanical significance of pneumatization in the long bones of birds. Zoological Journal of the Linnean Society. 2000;130(4):499-510. Doi: 10.1111/j.1096-3642.2000.tb02198.x

22. Veladiano IA, Banzato T, Bellini L, Montani A, Catania S, Zotti A. Computed tomographic anatomy of the heads of blue-and-gold macaws (Ara ararauna), African grey parrots (Psittacus erithacus), and monk parakeets (Myiopsitta monachus). American journal of veterinary research. 2016;77(12):1346-56. DOI: 10.2460/ajvr.77.12.1346

23. Wild JM. The avian somatosensory system: a comparative view. Sturkie's Avian physiology. Elsevier. 2015;11(1):55-69. DOI: 10.1016/B978-0-12-407160-5.00005-1

24. Langlois I, Barrs VR, Dufresne PJ. Rhinitis due to Aspergillus pseudoviridinutans in an orange-winged Amazon parrot (Amazona amazonica). Medical mycology case reports. 2020;30:46-50. Doi: 10.1016/j.mmcr.2020.11.001.

25. Hanafy BG. Structural adaption of the nasal conchae of Eurasian common moorhen (Gallinula chloropus chloropus, Linnaeus, 1758)—Histomorphological study. Microsc Res Tech. 2021;84(9):2195-202. Doi: 10.1002/jemt.23778.

26. Pohlmeyer K, Kummerfeld N. Morphologie der Nasenhöhle und der nasen Nebenhöhlen sowie ihre klinische Bedeutung bei Grosspapageien. Kleintierpraxis. 1989;34:127-33.

27. Orosz S. Clinical respiratory anatomy. CABI Digital Library. 2016;247-53.

28. Yokosuka M, Hagiwara A, Saito TR, Aoyama M, Ichikawa M, Sugita S. Morphological and histochemical study of the nasal cavity and fused olfactory bulb of the brown-eared bulbul, Hysipetes amaurotis. Zoological science. 2009;26(10):713-21. Doi: 10.2108/zsj.26.713.

29. Piro A, Acosta Hospitaleche C. Skull anatomy of Wilson's storm-petrel Oceanites oceanicus (Hydrobatidae, Procellariiformes). Polar Biology. 2019;42(8):1501-10. Doi: 10.1007/s00300-019-02536-x.

30. Al-Rubaie NI and Kadhim, K. Anatomical Comparison of the Nasal Cavity in Adult Male and Female Cockatiel (Nymphicus Hollandicus). Acta Biology. 2023;94(3): 2023719.

31. Madkour F. Anatomical descriptions of the nasal cavity of the Aquatic and Non-aquatic birds. SVU-International Journal of Veterinary Sciences. 2019;2(2):101-10. Doi: 10.21608/svu.2019.14982.

32. Van Zeeland Y. Upper respiratory tract disease. BSAVA Manual of Avian Practice: BSAVA Library; 2018;299-316. Doi: 10.22233/9781910443323.20.

33. Moore BA, Oriá AP, Montiani-Ferreira F. Ophthalmology of psittaciformes: parrots and relatives. Wild and Exotic Animal Ophthalmology: Volume 1: Invertebrates, Fishes, Amphibians, Reptiles, and Birds. Springer. 2022; 3(12):349-91. Doi: 10.1007/978-3-030-71302-7_17.

34. Smallwood JE. A Guided Tour of Avian Anatomy. Millennium Pring Group. 2014;155-167.

35. Silva IA, Vieira LC, Mancini VRM, Faillace ACL, Santana MIS. Radiographic anatomy of the cockatiel (Nymphicus hollandicus) axial and appendicular skeleton. Anatomia, histologia, embryologia. 2020;49(2):184-95. Doi: 10.1111/ahe.12510.

36. Casteleyn C, Cornillie P, Van Cruchten S, Van den Broeck W, Van Ginneken C, Simoens P. Anatomy of the upper respiratory tract in domestic birds, with emphasis on vocalization. Anatomia, histologia, embryologia. 2018;47(2):100-9. Doi: 10.1111/ahe.12336.

37. Grist A. Poultry inspection: anatomy, physiology and disease conditions. CABI Digital Library. 2006;276-292.

38. Massari CHdAL, Silva AF, Magalhães HIR, Silva DRS, Sasahara THdC, Miglino MA. Anatomía Comparada de los Picos de Guacamayo Azul y Amarillo (Ara ararauna) y de Tucán Toco (Ramphastos toco). International Journal of Morphology. 2020;38(6):1591-6. Doi: 10.4067/S0717-95022020000601591.

39. Carril J, Tambussi CP, Rasskin-Gutman D. The network ontogeny of the parrot: Altriciality, dynamic skeletal assemblages, and the avian body plan. Evolutionary Biology. 2021;48:41-53. Doi: 10.1007/s11692-020-09522-w.

40. Monção-Silva RM, Ofri R, Raposo ACS, Libório FA, Estrela-Lima A, Oriá AP. Ophthalmic parameters of Blue-and-yellow Macaws (Ara ararauna) and Lear's Macaws (Anodorhynchus leari). Avian Biology Research. 2016;9(4):240-9. Doi: 10.3184/175815516X14725499175746.

41. Webb TJ, Gaston KJ. Geographic range size and evolutionary age in birds. Proc R Soc Lond B Biol Sci. 2000;267(1455):1843-50. DOI: 10.1098/rspb.2000.1219.

42. Vučićević M, Stevanović J, Šekler M, Resanović R, Stanimirović Z. Historical overview of methods for sex determination in birds. Veterinarski glasnik. 2016; 11(2):145-57. Doi: 10.2298/VETGL1604145V.

43. Ma S, Wang L, Liu Z, Luo X, Zhou Z, Xie J, et al. "One stone, two birds": engineering 2-D ultrathin heterostructure nanosheet BiNS@ NaLnF 4 for dual-modal computed

tomography/magnetic resonance imaging guided, photonic synergetic theranostics. Nanoscale. 2021;13(1):185-94. Doi: 10.1039/d0nr07590f.

44. Brühschwein A, Klever J, Wilkinson T, Meyer-Lindenberg A. DICOM standard conformance in veterinary medicine in Germany: A survey of imaging studies in referral cases. Journal of Digital Imaging. 2018;31:13-8. Doi: 10.1007/s10278-017-9998-x.

45. Wilhite R, Wölfel I. 3D Printing for veterinary anatomy: An overview. Anatomia, histologia, embryologia. 2019;48(6):609-20. Doi: 10.1111/ahe.12502.

46. Šljivic M, Pavlovic A, Kraišnik M, Ilić J, editors. Comparing the accuracy of 3D slicer software in printed enduse parts. IOP conference series: materials science and engineering. IOP Publishing. 2019;12(1):100-119. Doi: 10.1088/1757-899X/659/1/012082.

47. Constantinescu GM, Constantinescu IA. The updated international veterinary anatomical and embryological nomenclatures. Journal of Veterinary Science and Animal Husbandry. 2013;1(2):1-3. Doi: 10.15744/2348-9790.1.e201.

How to cite this article
Alizadeh S, Hosseinchi MR, Esmaeilnejad R. Radioanatomical Study of the Rose-Ringed Parakeet (Psittacula Krameri) Head Based on the Findings of Computed Tomography Scanning. Iran J Vet Sci Technol. 2025; 17(3): 47-60.
DOI: https://doi.org/10.22067/ijvst.2025.89892.1422
URL:https://ijvst.um.ac.ir/article_47076.html